Ordering Tendencies in Pd-Pt, Rh-Pt, and Ag-Au Alloys

Z.W. Lu and B.M. Klein
Department of Physics
University of California
Davis, CA 95616
and
A. Zunger
National Renewable Energy Laboratory
Golden, CO 80401

(Submitted October 7, 1994; in revised form November 9, 1994)

First-principles quantum-mechanical calculations indicate that the mixing enthalpies for Pd-Pt and Rh-Pt solid solutions are negative, in agreement with experiment. Calculations of the diffuse-scattering intensity due to short-range order also exhibits ordering tendencies. Further, the directly calculated enthalpies of formation of ordered intermetallic compounds are negative. These ordering tendencies are in direct conflict with a 1959 prediction of Raub that Pd-Pt and Rh-Pt will phase-separate below ~760 °C (hence their mixing energy will be positive), a position that has been adopted by all binary alloy phase diagram compilations. The present authors predict that $Pd_{1-x}Pt_x$ will order in the $L1_2$, $L1_0$, and $L1_2$ structures ([001] superstructures) at compositions $x = \frac{1}{4}, \frac{1}{2}$, and $\frac{3}{4}$, respectively, while the ordered structures of $Rh_{1-x}Pt_x$ are predicted to be superlattices stacked along the [012] directions. While the calculated ordering temperatures for these intermetallic compounds are too low to enable direct growth into the ordered phase, diffuse-scattering experiments at higher temperatures should reveal ordering rather than phase-separation characteristics (i.e., off-Γ peaks). The situation is very similar to the case of Ag-Au, where an ordering tendency is manifested both by a diffuse scattering intensity and by a negative enthalpy of mixing. An experimental reexamination of Pd-Pt and Rh-Pt is needed.

1. Introduction

In 1959, Raub[1] suggested the existence of miscibility gaps in the Pd-Pt and Rh-Pt systems with fairly high maximum miscibility gap temperatures of 770 and 760 °C, respectively. He inferred these results from the assumed correlation between the maximum miscibility gap temperature and the difference in melting points of the constituents and from the experimentally observed miscibility gaps in similar alloys, such as Pd-Rh, Ir-Pt, and Ir-Pd.[1] Attempts to observe these miscibility gaps have, however, consistently failed.[2-5] In agreement with the conjecture of Raub, tight-binding *d*-band only alloy theories[6] predicted phase-separation for all *d*-electron-rich alloys, e.g. the late transition metal alloys (because the anti-bonding states are partially occupied). That this is not a compelling argument is clear from the fact that Ni-Pt orders strongly despite its high *d*-electron count. The reason for the failure of such arguments was recently clarified.[7] Phenomenological theories[8,9] are not clear on whether Pd-Pt and Rh-Pt should phase-separate or order: Miedema's model[8] predicts $\Delta H \approx +(1 \text{ to } 3)$ kJ/mol for Pd-Pt and $\Delta H \approx -(2 \text{ to } 3)$ kJ/mol for Rh-Pt, both values being close to the limit of accuracy of the model. Thus, neither experiment[2-5] nor simple phenomenological theories[8] shed light on whether these systems order or not. Yet, all phase-diagram compilations,[10-15] including the latest assessments by Massalski et al.[13] and Okamoto,[14,15] have adopted Raub's view, labeling Pd-Pt and Rh-Pt as phase-separating (miscibility gap) systems.

First-principles quantum mechanical stability calculations in conjunction with cluster expansions[16] offer an alternative method to the phenomenological approaches.[8,9] Here, note that such calculations[7] predict Pd-Pt and Rh-Pt to exhibit ordering rather than phase separating at low temperatures. This conclusion comes from the first-principles quantum mechanical calculations[7] backed up by experimental evidence,[17-19] which seems to have been largely overlooked by the alloy phase diagram community. The situation in Pd-Pt and Rh-Pt systems is very similar to that in Ag-Au where an ordering tendency[20] was recognized by ample experiments[21-24] and theoretical calculations[25-30] despite the fact that the ordering temperatures[24,30] are too low to actually grow ordered compounds. An experimental reexamination of the phase stability of Pd-Pt and Rh-Pt is thus needed.

The following gives a brief account of the theoretical strategy and then presents the results and discussion. For comparison and as a "sanity test," parallel calculations are also conducted for Pd-Rh, which is known experimentally[1,31,32] and theoretically[7,33-35] to phase separate. In the Rh-Pd-Pt triangle, Pd-Rh should phase separate (in agreement with experiment), but Pd-Pt and Rh-Pt should order (in distinction to current phase-diagram assessments).

2. Method of Calculation

2.1 Cluster-Expanding Lattice Quantities

Short- and long-range order (SRO and LRO) in binary $A_{1-x}B_x$ systems can be interpreted in terms of spin-$\frac{1}{2}$ lattice models in which each lattice site i ($i = 1, \ldots, N$) is labeled by a spin variable, $\hat{S}_i$, taking on the value $-1(+1)$ if site i is occupied by atom $A(B)$. The excess energy $\Delta E(\sigma,V)$ of any of the 2^N configurations σ obtained by occupying N sites by A or B is:

$$\Delta E(\sigma,V) = E(\sigma,V) - [(1-x)E_A(V_A) + xE_B(V_B)] \qquad \text{(Eq 1)}$$

The excess energy in Eq 1 depends on the volume, V, and is defined with respect to the energies of equivalent amounts of the pure solids A and B at their respective equilibrium volumes V_A and V_B. The low-temperature ground state structures of a given lattice type are then interpreted as the configurations σ that give the lowest $\Delta E(\sigma,V_\sigma)$ at the equilibrium volume V_σ. For phase-separating systems (miscibility gap) $\Delta E(\sigma,V)$ are positive for all structures, while for an ordering system, $\Delta E(\sigma,V)$ are negative for at least the ground-state structures.

Advances in the electronic structure theory[36] now enable practical and accurate quantum-mechanical calculations of the total energy of simple configurations σ:

$$E_{\mathrm{direct}}(\sigma,V) = \frac{\langle\Psi|\hat{H}|\Psi\rangle}{\langle\Psi|\Psi\rangle} \qquad \text{(Eq 2)}$$

where H and Ψ are the Hamiltonian and wave function of the electronic system. In practice, most calculations are performed using the density functional formalism,[37,38] as implemented numerically by, for instance, the highly precise, full-potential, linearized augmented plane wave (LAPW) method.[39,40] Such calculations include electrostatic, ionic, and exchange-correlation effects. They avoid tight-binding or spherical-potential approximations and account for metallic, ionic, and covalent bonding. However, since quantum-mechanical calculation of an astronomic number of configurational energies $\Delta E(\sigma,V)$ is prohibitive, one approach is to perform such a ground state search by expanding Eq 1 in a finite Ising-like cluster expansion (CE):

$$E_{\mathrm{CE}}(\sigma,V) = \sum_f D_f J_f(V)\bar{\Pi}_f(\sigma) \qquad \text{(Eq 3)}$$

where $J_f(V)$ are volume-dependent interaction energies of some basic lattice figures f (e.g., nearest-neighbor pairs, next neighbor pairs, triangles, etc.) as shown in Fig. 1. Their coordinates are defined in Table 1. The lattice averaged spin products $\Pi_f(\sigma)$ are the product over the figure f of the variables $\hat{S}_i$, averaged over all symmetry equivalent figures of the lattice. All of the terms on the right-hand side of Eq 3 are trivially determined geometrical quantities, with the exception of J_f, the effective interaction energies. Since $\{\Pi_f(\sigma)\}$ is a complete, orthonormal set of polynomials, the expansion Eq 3 is exact,[41] if not truncated. In practice, one hopes that this series converges reasonably rapidly so only ~$O(10)$ interaction are retained (the first few pair interactions, as well as many-body

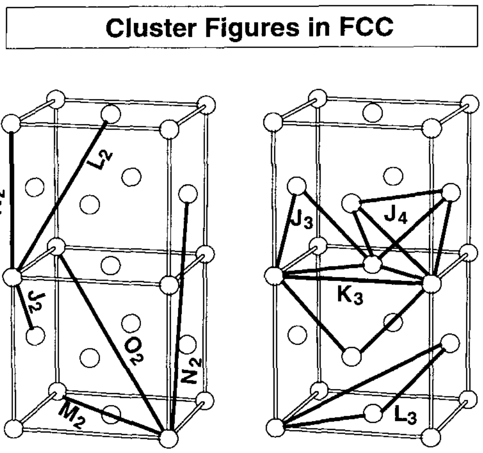

Fig. 1 Atomic figures used in the cluster expansion, which include pair figures, three-body figures, and four-body figures. Table 1 defines the figure coordinates.

Table 1 Definition of the Figures f Used in Cluster Expansion in Terms of the Vertices of the fcc Structure

Figure type	Designation	Vertices	Pd-Pt	Rh-Pt	Pd-Rh	Ag-Au
Empty	J_0	..	–28.2	–11.6	65.0	–43.41
Point	J_1	(000)	–3.1	4.2	1.9	1.95
Pairs	J_2	(000),(110)	22.6	43.2	–49.2	41.10
	K_2	(000),(200)	–0.7	0.1	0.4	0.71
	L_2	(000),(211)	10.9	–2.1	–9.9	3.65
	M_2	(000),(220)	–1.0	8.3	10.4	–0.48
	N_2	(000),(310)	...	...	...	–0.03
	O_2	(000),(222)	...	...	..	–0.89
Triplets	J_3	(000),(110),(101)	3.5	–6.6	0.7	–0.56
	K_3	(000),(110),(200)	. .	...	...	–2.22
	L_3	(000),(110),(211)	...		...	0.89
Quadruplets	J_4	(000),(110),(101),(011)	0.3	0.7	–3.9	–0.31

Note: Vertices are in units of $\frac{a}{2}$, where a is the lattice parameter. See Fig. 1. The effective $T = 0$ cluster interactions $D_f J_f$ (in meV/atom) at $x = \frac{1}{2}$ [or corresponding to $V = (V_A + V_B)/2$], are listed. The dominant negative (positive) J_2 denote phase-separating (compound-forming) interactions. One meV/atom equals 9.649×10^{-2} kJ/mol.

terms). If the series Eq 3 converges after M terms, one can calculate an equivalent number of interaction energies $\{J_f(V)\}$ by equating Eq 2 with Eq 3. For example, the simplest, direct inversion gives

$$D_f J_f(V) = \sum_{\sigma}^{M} \Delta E_{\mathrm{direct}}(\sigma, V)[\overline{\Pi}_f(\sigma)]^{-1} \qquad \text{(Eq 4)}$$

which can be obtained once one has performed self-consistent quantum-mechanical calculations on M different A_nB_m ordered structures. These structures do not have to be ground state structures. In fact, any collection of M hypothetical configurations (that have a nonsingular determinant in Eq 3) will do. Using Eq 4, extract a set of interaction energies $\{J_f\}$ from a set of total energies $\{E_{\mathrm{direct}}(\sigma, V)\}$. Convergence is examined by the ability of these M interaction energies to reproduce via Eq 3 the quantum-mechanically calculated energies of other configurations. This approach recently was reviewed.[16] Since the underlying quantum-mechanical calculations of $\Delta E_{\mathrm{direct}}(\sigma, V)$ automatically includes atomic size effects, charge-transfer, atomic displacements, exchange-correlation, and covalency, all of these factors are also encoded in the ensuing J_f.

Having obtained a converged set of interactions, the $T = \infty$ enthalpy of mixing of the random alloy can be readily evaluated. Denoting a configurational average for the random (R) state by angular brackets $\langle\rangle_R$, then:

$$\Delta_{\mathrm{mix}}H(x) = \sum_f D_f J_f \langle\overline{\Pi}_f\rangle_R = \sum_f D_f J_f (2x-1)^{k_f} \qquad \text{(Eq 5)}$$

where $\langle\overline{\Pi}\rangle_R = (2x-1)^{k_f}$, and k_f is the number of vertices in figure f (e.g., $k_f = 2$ for pair, 3 for triangles). The enthalpy of formation of ordered compounds is obtained by evaluating Eq 3 at the volume V_σ (as well as the appropriate external and internal coordinates) that minimizes $E(\sigma, V)$; i.e., $\Delta_f H(\sigma) = \Delta E(\sigma, V_\sigma)$. The ordering energy, $-\delta E_{\mathrm{ord}}(\sigma)$, is defined as the difference between the enthalpy of formation $\Delta_f H(\sigma)$ of an ordered configuration σ and the enthalpy of mixing $\Delta_{\mathrm{mix}}H(x)$ of a random alloy at the same composition x:

$$\delta E_{\mathrm{ord}}(\sigma) = \sum_f D_f J_f [\overline{\Pi}_f(\sigma) - (2x-1)^{k_f}] \qquad \text{(Eq 6)}$$

The order-disorder transition temperature thus can be estimated using the mean-field formula $-\delta E_{\mathrm{ord}} = kT_c[x \ln x + (1-x)\ln(1-x)]$, where on the right-hand side an ideal entropy of mixing is assumed. More accurate values of T_c can be calculated applying either the cluster-variational method[42] (CVM) or Monte-Carlo simulation[43] to the present set of interaction energies $\{J_f\}$. In these approaches, $\Delta_f H$ and $\Delta_{\mathrm{mix}}H$ are evaluated at finite temperatures so that effects of imperfect ordering (in $\Delta_f H$ or imperfect randomness in $\Delta_{\mathrm{mix}}H$) are included. Here, subject the effective interactions $\{J_f\}$ to a Monte-Carlo simulated annealing treatment,[43-45] which gives (a) the $T = 0$ LRO ground states (on a finite cell), (b) the order-disorder transition temperature T_c, and (c) the SRO diffuse-scattering map at a fixed temperature. Monte Carlo simulated annealing was performed in the canonical ensemble at a fixed concentration with the transition temperature being calculated from the discontinuity in the internal energy as a function of temperature and the ground state determined by the state of the simulation at a temperature where all configurational changes proved to be energetically unfavorable.[*]

The Warren-Cowley SRO parameter[46] for the Nth atomic shell at distance R_{lmn} from the origin is:

$$\alpha_{\mathrm{SRO}}(R_{lmn}) = \frac{\langle\overline{\Pi}_{0,N}\rangle - q^2}{1 - q^2} \qquad \text{(Eq 7)}$$

where $q = 2x - 1$, and the angular bracket denotes a configurational average. Note that $\alpha_{\mathrm{SRO}}(0) \equiv 1$ by definition. The Fourier transform of the real-space SRO is $\alpha_{\mathrm{SRO}}(\mathbf{k})$, which is proportional to the diffuse intensity due to SRO. Its value depends on the number of N_R of real-space shells used in the transform:

$$\alpha_{\mathrm{SRO}}(\mathbf{k}, N_R) = \sum_{N}^{N_R} \alpha_{\mathrm{SRO}}(R_{lmn}) e^{i\mathbf{k} R_{lmn}} \qquad \text{(Eq 8)}$$

For a binary alloy with a small lattice mismatch such as the systems studied here, the peak positions in reciprocal-space of high-temperature $\alpha(\mathbf{k})$ usually indicate the type of low-temperature order structure; i.e., phase-separating systems have peak position at the zone center the $\Gamma = \langle 000\rangle$ point, while ordering systems have peak positions off the Γ point. See Ref. 47 for a more complete discussion of the SRO versus LRO behaviors.

2.2 Calculating the Cluster Expansion Interaction Energies

The excess energy $\Delta E_{\mathrm{direct}}(\sigma, V)$ vs volume V for 12 ordered structures each in Pd-Pt, Pd-Rh, Rh-Pt, and Ag-Au were calculated. The structures are defined in Ref. 48. The total energies were calculated by self-consistently solving the effective Schrödinger equation (in atomic units: $m_e = \frac{1}{2}$, $e^2 = 2$, $\hbar = 1$)

$$\left\{-\nabla^2 + \sum_{\mu} \frac{2Z_\mu}{|\mathbf{R}_\mu - \mathbf{r}|} + \int \frac{2\rho(\mathbf{r}')}{|\mathbf{r} - \mathbf{r}'|} d\mathbf{r}' + \frac{\partial E_{\mathrm{xc}}[\rho]}{\partial \rho}\right\} \qquad \text{(Eq 9)}$$

$$\psi_i(\mathbf{r}) = \varepsilon_i \psi_i(\mathbf{r})$$

where $\rho(\mathbf{r}) = \Sigma_i \psi_i^*(\mathbf{r})\psi_i(\mathbf{r})$ is the charge density, $E_{\mathrm{xc}}[\rho]$ is the total exchange and correlation energy, and $\mathbf{R}_\mu$ are position coordinates of atom μ with atomic number Z_μ. The present authors use the local density description[37,38] for $E_{\mathrm{xc}}[\rho]$, for which they use the functional of Wigner[49] for Pd-Rh, Pd-Pt, and Pt-Rh and of Ceperley and Alder[50] as parameterized by Perdew and

---

[*] A Monte Carlo cell size of $16^3 = 4096$ atoms (with periodic boundary conditions) was used In the calculation of $\alpha_{\mathrm{SRO}}(R_{lmn})$ and $\alpha_{\mathrm{SRO}}(\mathbf{k}, N_R)$, 500 Monte Carlo steps per site are used to equilibrate the system (which is initialized in a completely random state), and subsequently, averages are taken over 100 Monte Carlo steps per site The ground state structures are searched among a set of ~65 000 structures that have less than 16 atoms per unit cell for Pd-Pt and Rh-Pt, while the ground state structures are found using Monte-Carlo simulated annealing approach for Ag-Au system.

Table 2 LAPW-Calculated Enthalpies of Formation in the meV/atom of the $A_{1-x}B_x$ Intermetallics

Structure	$Pd_{1-x}Pt_x$	$Rh_{1-x}Pt_x$	$Pd_{1-x}Rh_x$	$Ag_{1-x}Au_x$
fcc (*A*)	0	0	0	0
$L1_2(A_3B)$	–30.4	–20.4	66.8	–43.4
$D0_{22}(A_3B)$	–22.1	–25.2	69.0	–42.3
$\beta1(A_3B)$	–28.2	–10.0	72.5	–40.8
$L1_0(AB)$	–39.5	–16.5	82.4	–59.7
$L1_1(AB)$	–29.1	–3.9	79.0	–40.0
"40" (*AB*)	–32.1	–29.5	70.7	–55.3
$Z2(A_2B_2)$	–24.7	–0.4	35.1	–28.8
$\beta2(AB_2)$	–30.4	–4.3	64.2	–40.0
$D0_{22}(AB_3)$	–29.1	–13.0	63.8	–41.0
$L1_2(AB_3)$	–35.1	–10.8	85.0	–44.0
fcc (*B*)	0	0	0	0
δE	1.1	2.1	7.1	0.6
$\Delta_{mix}H(\frac{1}{2})$	–28.2	–11.6	65.0	–43.4
δE_{ord}	–11.3	–17.9		–16.3
T_c^{MF}	189	300	.	273

Note: Various structures are defined in Ref. 48. One meV/atom equals 9.649 × 10^{-2} kJ/mol. The cluster expansion fitting errors δE are given. This table gives the calculated, high-temperature enthalpies of mixing of the disordered alloys at $x = \frac{1}{2}$ Also given are the ordering energies of Pd-Pt ($L1_0$), Rh-Pt ("40"), and Ag-Au ($L1_0$) and the corresponding estimated transition temperatures (in Kelvin) using the simple mean-field formula $\delta E_{ord} = kT_c^{MF}[x \ln x + (1-x)\ln(1-x)]$.

Zunger[51] for Ag-Au. Equation 9 was solved self-consistently by the full-potential linearized augmented plane wave (LAPW) method.[39,40] Any shape approximation (e.g., muffin-tin) to the potential and charge density or any elimination of a subset of states (e.g., the pseudopotential approximation) is avoided. The core states are treated fully relativistically while the valence states are treated scalar relativistically. The spin-orbit coupling for the valence electrons can be treated in a second variational procedure. The spin-orbit effects on the enthalpy of formation is, however, rather small, e.g., it changes ΔH in the $L1_0$ structure for Ag-Au by less than 1.5 meV/atom. All matrix elements between basis functions are calculated numerically with no approximation. The calculation is fully self-consistent. Core states are also treated self-consistently (i.e., no frozen core approximation), but using only the spherical piece of the potential. To obtain highly precise results, a **k** point sampling is used that is geometrically equivalent in the compound and its pure constituents. For example, by use of such a set, the total energy of A_3A in the $L1_2$ or $D0_{22}$ crystal structures are all equal to the fcc value. In practice, sets of **k**-points are used that are equivalent to 408 fcc special **k**-points[52] for Ag-Au (increasing **k**-points from 60 to 408 alters ΔH by less 1.6 meV/atom) and 60 for the other systems. Also used is a large basis set cutoff of $R_{MT}K_{max} = 9.0$, which corresponds to ~90 LAPW/atom.

Having solved Eq 9 self-consistently, one obtains the total energy as:

$$E_{direct}(\sigma, V) = \sum_i <\psi_i| -\nabla^2 |\psi_i> + \frac{1}{2}\sum_{\mu,\nu} \frac{2Z_\mu Z_\nu}{|\mathbf{R}_\mu - \mathbf{R}_\nu|}$$

$$+ \sum_\mu \int \rho(\mathbf{r}) \frac{-2Z_\mu}{|\mathbf{R}_\mu - \mathbf{r}|} + \frac{1}{2}\int\int \frac{2\rho(\mathbf{r})\rho(\mathbf{r}')}{|\mathbf{r} - \mathbf{r}'|} d\mathbf{r}d\mathbf{r}' + E_{xc} \qquad \text{(Eq 10)}$$

where the terms are kinetic energy, ion-ion, electron-ion, electron-electron Coulomb energy, and exchange-correlation energy. For structures possessing external and internal degrees of freedom (e.g., *c/a* relaxation in the $L1_0$ structure), we optimize these parameters (atomic relaxation) to achieve the lowest total energy. Such relaxation was previously[53] shown to have a significant effect on ΔH of compounds with size-mismatched constituents. For example, in NiPt and NiAu, relaxation lowers $\Delta H(L1_0)$ by –18 (out of –96) and –20 (out of 77) meV/atom, respectively. In the disordered 50%-50% phase of these alloys, the energy lowerings due to relaxation are –54 and –68 meV/atom, respectively. Since relaxation is different in ordered vs disordered states, it has a significant effect on ordering energy δE_{ord}. For example, for NiAu without relaxation $\delta E_{ord}(L1_0) = -96$ meV/atom while with relaxation $\delta E_{ord}(L1_0) = -48$ meV/atom. The relaxation can even change the sign of ΔH (see examples of this in Ref. 48). For the present systems with relative small lattice mismatch, the effect of relaxation is small, e.g., it lowers $\Delta H(L1_0)$ by 1.8 meV/atom for Ag-Au. The estimated LAPW errors are approximately ±2 meV/atom for Ag-Au and larger (approximately ±10 meV/atom) for the other systems.

The formation enthalpies of Eq 1, $\Delta E_{direct}(\sigma, V_\sigma) = \Delta_f H$, at the equilibrium volume V_σ, are given in Table 2. Next, the directly calculated excess energies $\Delta E_{direct}(\sigma, V)$ are used to extract $\{J_f\}$ via Eq 3. Eight to twelve figures described in Table 1 and Fig. 1 are used. For Ag-Au, the 12 interaction $\{J_f\}$ are obtained from a more extended set of 18 structures (see Ref. 45) with average fitting error of 0.6 meV/atom. The convergence is then checked by the ability of these $\{J_f\}$ to predict 14 other structures that are not used to extract $\{J_f\}$. Comparing with direct LAPW calculated values, an average prediction error of 1.0 meV/atom is found with the maximum error being 1.8 meV/atom, smaller than the estimated LAPW error (±2 meV/atom) for Ag-Au. The average fitting errors for other systems are larger, and they are listed in Table 2.

Determination of the $T = 0$ ordered ground state structures involves three steps. (1) Verify that the structures have negative

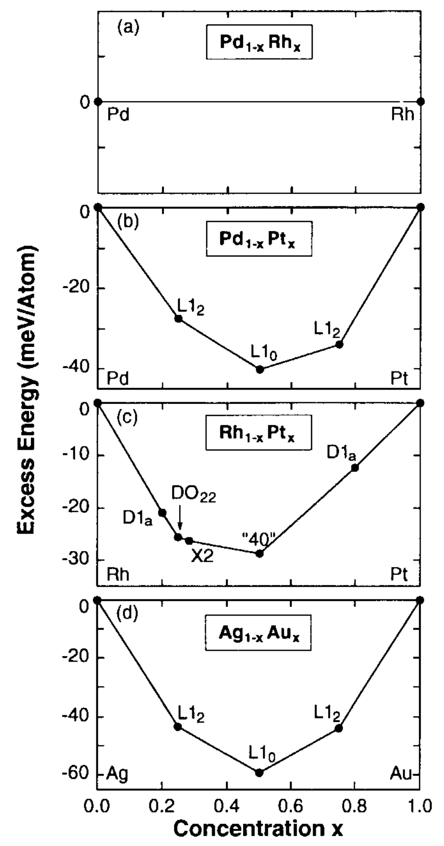

Fig. 2 Predicted $T = 0$ ground states (closed circles) as a function of composition for **(a)** Pd-Rh, **(b)** Pd-Pt, **(c)** Rh-Pt, and **(d)** Ag-Au systems. One meV/atom equals 9.649×10^{-2} kJ/mol.

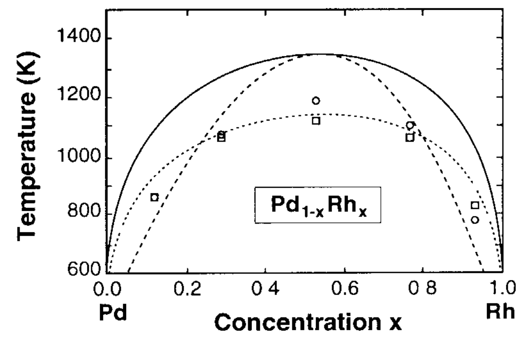

Fig. 3 CVM calculated (lines) and measured (circles from Ref. 32 and squares from Ref. 31) phase diagram of $Pd_{1-x}Rh_x$. The solid line is the binodal, the dashed line is the spinodal, and the dotted line is the calculated binodal corresponding to a ~12% reduction in $\Delta_f H$ (see text).

formation energy $\Delta_f H < 0$ (otherwise phase separation would be energetically preferred). (2) At each composition, find the structure with the lowest $\Delta H(\sigma)$ (for example using Monte Carlo simulated annealing method). (3) Determine if $\Delta H(\sigma)$ lies below the tie line connecting the neighboring lowest energy structures in the energy versus composition diagram. To illustrate this step, let σ, α, and β denote three configurations with concentration of *B* atoms x_σ, x_α, and x_β in the order $x_\alpha \le x_\sigma \le x_\beta$. If $\Delta_f H(\sigma)$ is larger than the linear average of $\Delta_f H(\alpha)$ and $\Delta_f H(\beta)$, that is if

$$\Delta_f H(\sigma) > \frac{x_\sigma - x_\beta}{x_\alpha - x_\beta}\Delta_f H(\alpha) + \frac{x_\sigma - x_\alpha}{x_\beta - x_\alpha}\Delta_f H(\beta)$$

then configuration σ does not belong to the ground state because a mixture of the equilibrium phases α and β would have a lower energy. The ground states can thus be represented by vertices in an energy versus composition diagram, the straight lines connecting vertices (ground states) in such a diagram are the lowest possible energy at a particular composition for the alloy system.

3. Results and Discussion

3.1 Low-Temperature Long-Range Order

Pd-Rh. This method was first tested for a known phase-separating system—Pd-Rh. Note first from Table 2 that the calculated enthalpies of formation, $\Delta_f H$, for Pd-Rh are all positive, implying phase-separating behavior. Second, the dominant nearest neighbor interaction J_2 (Table 1) is negative, also implying phase-separation. Third, its ground state line corresponds to a trivial horizontal line (see Fig. 2a). The temperature versus composition phase diagram of Pd-Rh was previously calculated[7] using the CVM. The calculated miscibility gap temperature (see Fig. 3) is in reasonable agreement with experiment[31,32] (overestimating it by ~160 K) and other theoretical calculations.[33-35] Note that in the present calculation no empirical data or parameter adjustment is used, and vibrational and coherency effects are neglected. Figure 3 also shows that the calculated phase diagram can be brought into perfect agreement with experiment if LAPW-calculated excess enthalpies $\Delta_f H$ of the input structures are lowered by a reasonable error margin of 12%.

Pd-Pt. In contrast to the Pd-Rh system, Pd-Pt, Rh-Pt, and Ag-Au all exhibit negative enthalpies of formation $\Delta_f H$ for the 12 structures listed in Table 2, thus unequivocally indicating ordering rather than phase-separating tendencies. Concomitantly, the dominant interaction energies, J_2 (Table 1), are positive, indicating ordering tendencies. The predicted $T = 0$ ground states for $Pd_{1-x}Pt_x$ are shown in Fig. 2(b), where the vertices represent the $L1_2$, $L1_0$, and $L1_2$ for $x = \frac{1}{4}, \frac{1}{2}$, and $\frac{3}{4}$, respectively. Figure 4(a) and (b) show the crystal structures of these ground states. These ordered structures are characterized by a reciprocal-space wave-vector of $\mathbf{k} = \frac{2\pi}{a}$ <001>, where *a* is the lattice constant of the underlying fcc lattice. Section 3.3 shows that the peaks of the calculated high-temperature diffuse-scattering intensity due to SRO also occur at these wave vectors.

Rh-Pt. Figure 2(c) shows the predicted $T = 0$ ground states for $Rh_{1-x}Pt_x$. They are all superlattices along the [012] direction. These are denoted the $D1_a$, $D0_{22}$, $X2$ (Au_5Mn_2 type), "40," and

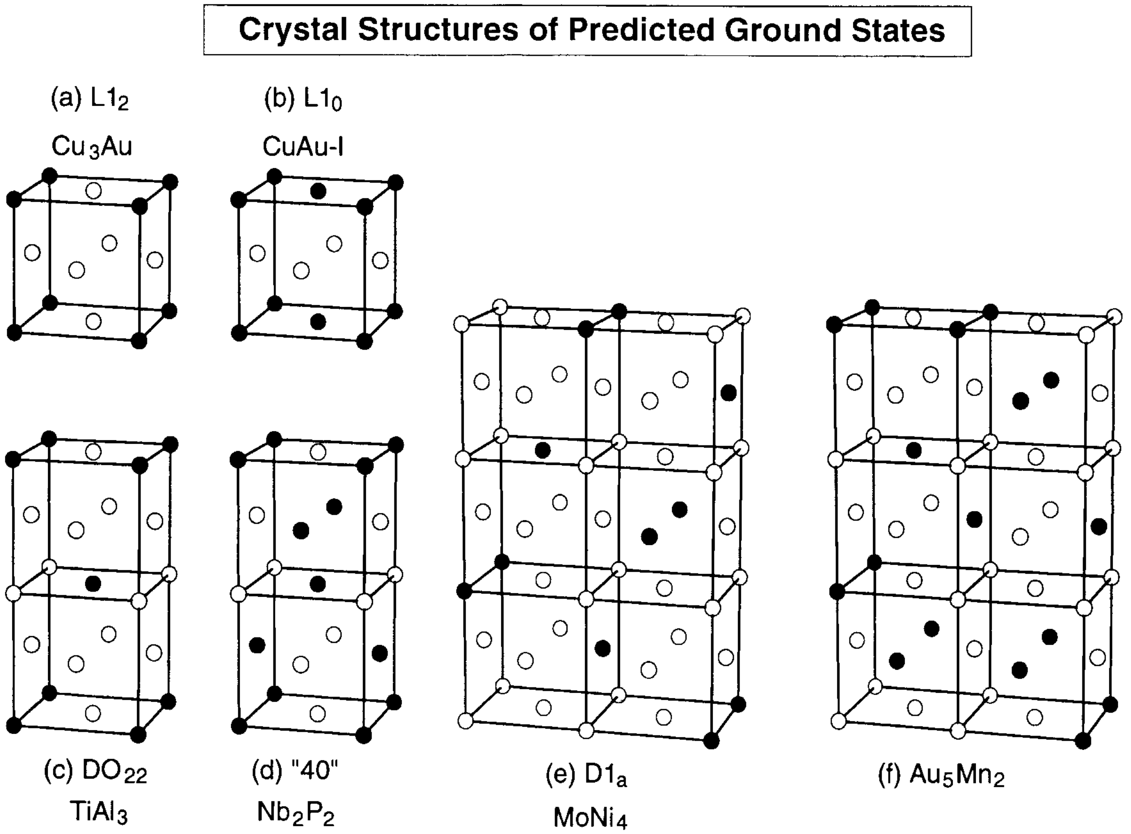

Fig. 4 Crystallographical structures of the predicted $T = 0$ ground states. Figure 2 of Pd-Pt [$L1_2$ (a) and $L1_0$ (b)], Rh-Pt [$D1_a$ (e), $D0_{22}$ (c), "40" (d), and $X2$ (f)], and Ag-Au [$L1_2$ (a) and $L1_0$ (b)] systems.

$D1_a$ for $x = \frac{1}{5}, \frac{1}{4}, \frac{2}{7}, \frac{1}{2}$, and $\frac{4}{5}$, respectively. These crystal structures are shown in Fig. 4(c) to (f). Many of these predicted ground states ($D1_a$ and Au_5Mn_2) are absent from out input set (used to extract interaction parameters) since such structures were not suspected to be stable. These ordered structures are characterized by a reciprocal-space wave-vector of $\mathbf{k} = \frac{2\pi}{a} <1\frac{1}{2}0>$. Section 3.3 shows that these indeed correspond to the maxima in the calculated diffuse scattering intensity. Magri et al.[54] and Wolverton and Zunger[55] have shown that the ground state structures of fcc lattice having only point-ion interactions are $D0_{22}$, "40," and $D0_{22}$. It is thus possible that small stabilizing negative enthalpy of formation found in Rh-Pt is due to the charge transfer effect.

Ag-Au. Similar to the Pd-Pt system, the predicted $T = 0$ ground states for $Ag_{1-x}Au_x$ (Fig. 2d) are also $L1_2$, $L1_0$, and $L1_2$ for $x = \frac{1}{4}, \frac{1}{2}$, and $\frac{3}{4}$, respectively. These are shown in Fig. 2(d); the ground state lines are fairly symmetric with respect to $x = \frac{1}{2}$. This symmetry is also seen in section 3.2 (Fig. 5d) in the calculated and measured mixing energy for the random alloy at high temperatures.

The order-disorder transition temperatures T_c for the ground state can be estimated from the ordering energy of Eq 6 using the mean-field formula $\delta E_{\text{ord}} = kT_c^{\text{MF}}\,[x \ln x + (1-x)\ln(1-x)]$. Table 2 gives the T_c^{MF} for some of the ground states, e.g., the T_c^{MF} are 189, 300, and 273 K for the $L1_0$ (PdPt), "40" (Rh_2Pt_2), and $L1_0$ (AgAu). The more accurate Monte-Carlo simulated annealing procedure gives the corresponding $T_c^{\text{MC}} \approx 210$ K for the above compounds. At such low transition temperatures, the atomic diffusion rates are clearly too slow to actually form these ordered ground states. Only solid solution across the whole composition ranges are thus observed. Of course, the observation of solid solutions above T_c is consistent with both phase-separation or ordering at lower temperature. The present theory suggests unequivocally that the equilibrium structures should be ordered.

3.2 Mixing Energy of Disordered Alloys at Finite Temperatures

Figure 5 compares the calculated and available, experimental enthalpies of mixing[19,22,56] at finite temperatures. The calculated results were obtained using CVM for Pd-Rh, Pd-Pt, and Rh-Pt and Monte-Carlo simulations for Ag-Au (tetrahedron CVM gives a result that is within 3 meV/atom for Ag-Au). The positive sign of enthalpy of mixing for Pd-Rh (Fig. 5a) is consistent with its phase-separation behavior at low temperatures, while the negative signs of the enthalpies of mixing for Pd-Pt,

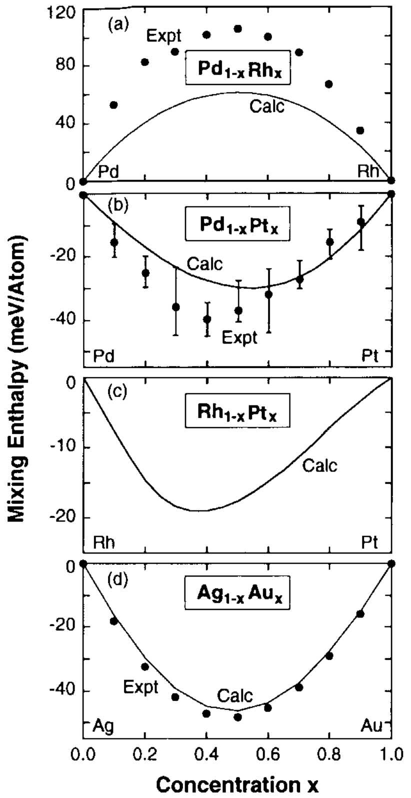

Fig. 5 Calculated and measured (where available) mixing energy for **(a)** $Pd_{1-x}Rh_x$ at $T = 1575$ K, **(b)** $Pd_{1-x}Pt_x$ at $T = 300$ K, **(c)** $Rh_{1-x}Pt_x$ at $T = 300$ K, and **(d)** $Ag_{1-x}Au_x$ at $T = 800$ K. The measured data are cited from Ref. 56 for Pd-Rh, Ref. 19 for Pd-Pt, and Ref. 22 for Ag-Au, while the statistical part of calculations was performed using CVM for Pd-Rh, Pd-Pt, and Rh-Pt and Monte-Carlo simulation for Ag-Au. One meV/atom equals 9.649×10^{-2} kJ/mol.

Rh-Pt, and Ag-Au indicate ordering tendencies of these alloys rather than phase separation.

Pd-Rh. Figure 5(a) compares the present calculated enthalpy of mixing[57] for Pd-Rh with experiment[56] at $T = 1575$ K.* The experimental values are consistently higher than the calculated values by nearly a constant factor of 1.7 (except for three points at the two ends, $x = 0.1, 0.2$, and 0.9). This is surprising because the present calculated phase diagram can be brought into nearly perfect agreement with experiment if one reduces (rather than increases) the calculated enthalpies of formation of the ordered structures $\Delta_f H$ by ~12% as shown in Fig. 3. It hence appears that the measured $\Delta_{mix}H$ of Ref. 56 is somewhat inconsistent with the measured phase diagram of Ref. 31 and 32 at least if the latter is interpreted via tetrahedron CVM. A careful reevaluation of the experimental data is therefore needed. A previous calculation by Wolverton et al.[34] (at $T = \infty$) gave a value of ~80 meV/atom (7.72 kJ/mol), which is between the present calculated value of 60.7 meV/atom (5.86 kJ/mol) and the experimental value of 104.5 meV/atom (10.08 kJ/mol).

Pd-Pt and Ag-Au. The calculated $\Delta_{mix}H(x)$ for Pd-Pt agrees reasonably well with experiment,[19] while for Ag-Au the agreement is excellent. Note that the calculated $\Delta_{mix}H(x)$ are consistently above experiment[22] by less than 2.7 meV/atom (0.26 kJ/mol) for Ag-Au. There were a few previous calculations[26] of $\Delta_{mix}H(x)$ of Ag-Au using the simple Connolly and Williams[58] procedure [i.e., extracting nearest neighbor interactions J_0, J_1, J_2, J_3, J_4 in Fig. 1 from total energy calculated on five ordered structures fcc (A), $L1_2$ (A_3B), $L1_0$ (AB), $L1_2(AB_3)$,

---

*Note that the volume-dependent J (and subsequent diffuse scattering intensity map due to SRO) here for Pd-Rh are slightly different from volume-independent ν extracted using the ε – G approach (Ref. 57) listed in Ref. 47.

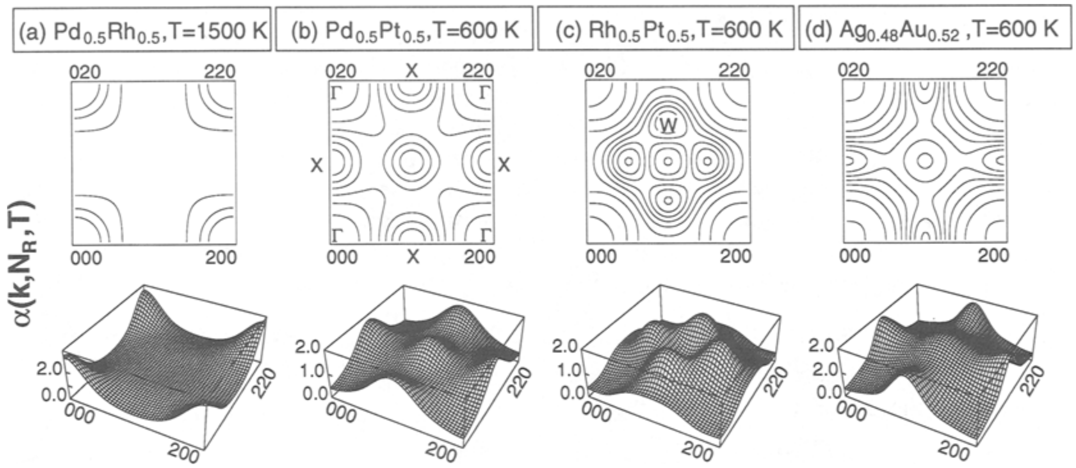

Fig. 6 Calculated diffuse scattering intensity due to short-range order a(**k**, N_R) for **(a)** $Pd_{0\ 5}Rh_{0\ 5}$ ($T = 1500$ K), **(b)** $Pd_{0\ 5}Pt_{0\ 5}$ ($T = 600$ K), **(c)** $Rh_{0\ 5}Pt_{0\ 5}$ ($T = 600$ K), and **(d)** $Ag_{0\ 478}Au_{0\ 523}$ ($T = 600$ K), $\alpha(\mathbf{k}, N_R)$ were Fourier synthesized using $N_R = 13$ real-space $\alpha(R_{lmn})$ (including $\alpha(R_{000}) \equiv 1$) Note that Pd-Rh has peak on the $\Gamma = \frac{2\pi}{a}$ <000> point indicating phase-separating behavior, while Pd-Pt, Rh-Pt, and Ag-Au all have off Γ peaks indicating ordering tendencies.

and fcc (B)]. They also achieved fair agreement with experiment.

Rh-Pt. There are no measured $\Delta_{mix}H$ data for solid solutions of Rh-Pt. However, the enthalpy of mixing of liquid $Rh_{1-x}Pt_x$ was recently estimated to be $\Delta_{mix}H^{L}(x) = -6x(1-x)$ kJ/mol, which was derived from measured liquidus and solidus[59] and according to a semiempirical model.[60] Thus, $\Delta_{mix}H^{L} = -1.50$ kJ/mol or −15.6 meV/atom at $x = \frac{1}{2}$. This is consistent in sign and magnitude of the present calculated enthalpy of mixing (−11.8 meV/atom or −1.15 kJ/mol when $T \rightarrow \infty$ and −17.6 meV/atom or −1.70 kJ/mol when $T = 300$ K) of solid solution. Hence, accurate measurements on mixing energies of solid solution for Rh-Pt is needed to compare with the present theoretical prediction in Fig. 5(c).

3.3 High-Temperature Short-Range Order

The calculated, high-temperature SRO diffuse intensities for Pd-Rh, Pd-Pt, Rh-Pt, and Ag-Au are shown in Fig. 6.

Pd-Rh. The calculated high-temperature SRO diffuse intensity for Pd-Rh (Fig. 6a) peaks at the Γ point indicating phase-separating behavior at low temperature, in agreement with the observed phase-diagram data. SRO measurements are unavailable.

Pd-Pt and Rh-Pt. Kidron[17] measured the SRO in a polycrystalline $Pd_{0.49}Pt_{0.51}$ sample annealed at 873 K. He found a negative $\alpha(R_{110}) = -0.10$ indicating an ordering tendency. Unfortunately, this work as well as the subsequent measurements of $\Delta_{mix}H(x)$[18,19] showing negative values seem to have largely been overlooked by phase-diagram compilations that characterized this system as having a miscibility gap. The present authors calculated $\alpha(R_{110}) = -0.040$ at $T = 873$ K for $Pd_{0.5}Pt_{0.5}$. Since the SRO parameters are very sensitive to the sample condition and heat treatment, careful SRO measurements on single crystal Pd-Pt and Rh-Pt samples are highly desirable. The predicted $\alpha(\mathbf{k})$ at $T = 600$ K for $Pd_{0.5}Pt_{0.5}$ and $Rh_{0.5}Pt_{0.5}$ are presented in Fig. 6(b) and (c), respectively, and are awaiting experimental comparison. The maximum diffuse intensities occur at the $X = \frac{2\pi}{a}<001>$ and $W = \frac{2\pi}{a}<0\frac{1}{2}1>$ points for $Pd_{0.5}Pt_{0.5}$ and $Rh_{0.5}Pt_{0.5}$, respectively, which corresponds to the wave vectors of their respective lower-temperature ordered ground states. Since the structure "40" rarely occurs in nature, it would be very interesting to see experimentally if the SRO indeed peaks at the $\frac{2\pi}{a}<0\frac{1}{2}1>$ points for $Rh_{0.5}Pt_{0.5}$.

Ag-Au. The short-range order in $Ag_{1-x}Au_x$ alloys was measured by a number of authors.[21,23,24] Recently, Schönfeld et al.[24] carefully measured the SRO at three different compositions, $x = 0.253$, 0.523, and 0.750, and found maxima at the wave vector $\frac{2\pi}{a}<001>$. These authors extracted composition dependent pair interaction energies from their measured real-space short-range order parameters $\alpha(R_{lmn})$ using the inverse Monte-Carlo method.[61] Their subsequently Monte-Carlo analysis using such interaction energies as input produced the same ground states and similar transition temperature as the present results. Figure 7 compares our calculated $\alpha(\mathbf{k})$ with experiment for $Ag_{0.477}Au_{0.523}$. The calculated maxima occur at the wave vector $\mathbf{k} = \frac{2\pi}{a}<001>$ (and its equivalent points) with intensity of 1.83. This is in close agreement with the experimental value of 1.75.

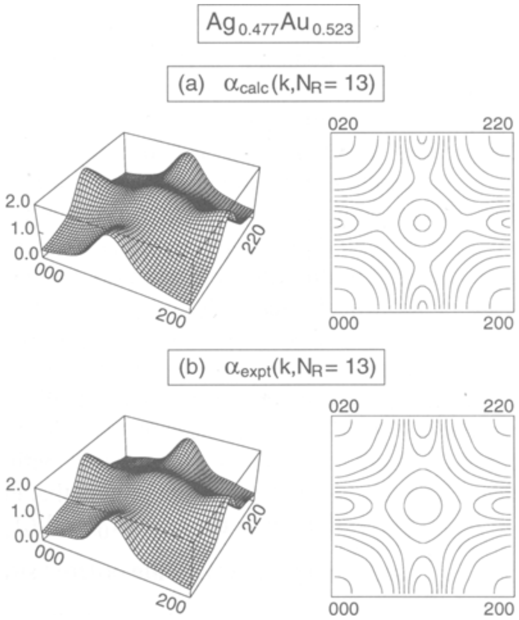

Fig. 7 Calculated **(a)** and experimental **(b)** (Ref. 24) diffuse scattering intensity due to short-range order $\alpha(\mathbf{k}, N_R)$ for $Ag_{0.477}Au_{0.523}$, which were Fourier synthesized using $N_R = 13$ real-space $\alpha(R_{lmn})$ (including $\alpha(R_{000}) \equiv 1$ for both experiment and theory). The calculation was done at $T = 600$ K, while the experiment was performed on a sample that was homogenized at $T = 1203$ K and later aged at $T = 502$ K.

The authors of Ref. 26 used a similar approach to the one employed here, except that the effective interaction energies of Eq 4 were extracted from only five, high-symmetry structures $\sigma = A(\text{fcc}), A_3B\,(L1_2), AB\,(L1_0), AB_3\,(L1_2)$, and B (fcc). Their interaction energies are limited to first nearest neighbors. Although this simple approach reproduces the $\Delta_{mix}H(x)$ well, it cannot correctly reproduce the shape and composition dependence of $\alpha(\mathbf{k})$. This is so because in this approach one ignores second neighbor interaction thus spuriously creating a degeneracy between the $T = 0$ energies of the $L1_2$ and $D0_{22}$ structures as well as between the $L1_0$ and "40" structures. Since this degeneracy survives at high temperatures, the calculated $\alpha(\mathbf{k})$ have flat maxima along the line connecting the two X points $\frac{2\pi}{a}<001>$ and $\frac{2\pi}{a}<011>$ (the $W = \frac{2\pi}{a}<0\frac{1}{2}1>$ point is in the middle).

4. Conclusion

Using a first-principles quantum-mechanical method (which properly includes the terms that were neglected by the previous theories, such as simplified tight-binding Hamiltonian models, neglect of relativistic effects and charge transfer effects), the present authors have shown that Pd-Pt and Rh-Pt binary alloy systems will order, rather than phase separate as assumed by many compilations of binary phase-diagram collections. However, the ordering temperatures for these two systems are rather low, similar to the Ag-Au systems, where the ordering propensity has been widely recognized. In the case of Pd-Pt, the present calculated mixing energy is in fair agreement with experiment, while for Ag-Au excellent agreement was found. The calculated diffuse intensity due to short-range order for Ag-Au is also in good accord with recent experiments. The present authors further predict that $Pd_{1-x}Pt_x$ as well as $Ag_{1-x}Au_x$ will order in the $L1_2$, $L1_0$, and $L1_2$ structures at $x = \frac{1}{4}, \frac{1}{2}$, and $\frac{3}{4}$, respectively, while ordered structures are in $Rh_{1-x}Pt_x$ are all superlattices stacked along the [012] directions. Since the ordering temperatures are so low (below the room temperature), these ordered phases may never be observed. However, peak positions in the measured SRO intensity would lend support to the existence of these ordered low-temperature LRO structures. Hence, accurate SRO measurements on single-crystal Pd-Pt and Rh-Pt as well as measured mixing energy for solid solution of Rh-Pt are highly desirable.

Acknowledgments

Z.W.L. and B.M.K. thank the support by the University Research Funds of the University of California at Davis. A.Z. thanks the support by the Office of Energy Research (OER) [Division of Materials Science of the Office of Basic Sciences (BES)], U.S. Department of Energy, under contract No. DE-AC36-83CH10093.

Cited References

1. E. Raub, *J. Less-Common Met., 1*, 3-18 (1959).
2. E. Raub and G. Falkenburg, *Z. Metallkd., 55*, 392-397 (1964).
3. V.E. Antonov, T.E. Antonova, I.T. Belash, E.G. Ponyatovshii, and V.I. Rashupkin, *Phys. Status Solidi (a), 78*, 137-146 (1983)
4. S.R. Bharadwaj, A.S. Kerkar, S.N. Tripathi, and S.R. Dharwadkar, *J. Less-Common Met., 169*, 167-172 (1991).
5. H. Noh, T.B. Flanagan, and Y. Sakamoto, *Scr. Metall. Mater., 29*, 445-450 (1993).
6. J. Van Der Rest, F. Gautier, and F. Brouers, *J. Phys. F, 5*, 2283 (1975); M. Cyrot and F. Cyrot-Lackmann, *J Phys F, 6*, 2257 (1976); G. Treglia and F. Ducastelle, *J. Phys. F, 17*, 1935 (1987); M. Sluiter, P. Turchi, and D. de Fontaine, *J. Phys. F, 17*, 2163 (1987).
7. Z.W. Lu, S.-H. Wei, and A. Zunger, *Phys. Rev. Lett., 66*(13), 1753-1756 (1991).

8 *Cohesion in Metals: Transition Metal Alloys*, F R. de Boer et al., Ed , North Holland, Amsterdam (1988).

9 D G. Pettifor, *New Sci., 110*(1510), 48-53 (1986).

10 R P Elliott, *Constitution of Binary Alloys, First Supplement*, Genium Publishing Corporation, Schenectady, NY, 748 (1965).

11. F.A. Shunk, *Constitution of Binary Alloys, Second Supplement*, Genium Publishing Corporation, Schenectady, NY, 607, 622 (1969).
12. W.G. Moffatt, *Handbook of Binary Phase Diagrams*, Genium Publishing Corporation, Schenectady, NY (1978).
13. T.B. Massalski, P.R. Subramanian, H. Okamoto, and L. Kacprzak, *Binary Alloy Phase Diagrams*, Vol 3, ASM International, Materials Park, OH, 3020, 3022, 3033-3034 (1990).
14. H. Okamoto, *J. Phase Equilibria, 12*(5), 617-618 (1991).
15. H. Okamoto, *J. Phase Equilibria, 13*(2), 223-224 (1992).
16. A. Zunger, in *Stat and Dynamics of Alloy Phase Transitions*, P.E.A. Turchi and A. Gonis, Ed., NATO ASI Series, Kluwer Academic Publishers, Dordrecht, The Netherlands (1994).
17. A. Kidron, *Phys. Lett. A, 25*, 112-113 (1967).
18. F.H. Hayes and O. Kubaschewski, *Met. Sci. J., 5*, 37 (1971).
19. J.B. Darby and K.M. Myles, *Metall. Trans., 3*, 653-657 (1972).
20. *Phase Diagrams of Binary Gold Alloys*, H. Okamoto and T.B. Massalski, Ed., ASM International, Metals Park, OH, 76 (1987).
21. N. Norman and B.E. Warren, *J. Appl. Phys., 22*, 483 (1951).
22. J.L. White, R.L. Orr, and R. Hultgren, *Acta Metall., 5*, 747-760 (1957).
23. K. Ziesemer, Ph.D. thesis, Universität Frankfurt, 1976.
24. B. Schönfeld, J. Traube, and G. Kostorz, *Phys. Rev. B, 45*(2), 613-621 (1992).
25. S.-H. Wei, A.A. Mbaye, L.G. Ferreira, and A. Zunger, *Phys. Rev. B, 36*, 4163 (1987).
26. K. Terakura, T. Oguchi, T. Mohri, and K. Watanabe, *Phys. Rev. B, 35*(5), 2169-2173 (1987); T. Mohri, K. Terakura, T. Oguchi, and K. Watanabe, *Acta Metall. Mater., 36*(3), 547-553 (1988); T. Mohri, K. Terakura, S. Takizawa, and J.M. Sanchez, *Acta Metall. Mater., 39*(4), 493-501 (1991); T. Mohri, S. Takizawa, and K. Terakura, *J. Phys. Condens. Matter, 5*, 1473-1480 (1993).
27. R.A. Johnson, *Phys. Rev. B, 39*(17), 12554-12559 (1989); *41*(14), 9717-9720 (1990).
28. G.J. Ackland and V. Vitek, *Phys. Rev. B, 41*(15), 10324-10333 (1990).
29. B.M. Klein and C.Y. Fong, in *Metallic Alloys: Experimental and Theoretical Perspectives*, J.S. Faulkner and R.G. Jordan, Ed., 291, Kluwer Academic Publishers, Dordrecht, The Netherlands (1994).
30. Z.W. Lu, B.M. Klein, and A. Zunger, manuscript in preparation.
31. E. Raub, H. Beeskow, and D. Menzel, *Z. Metallkd., 50*, 428 (1959).
32. J.E. Shield and R.K. Williams, *Scr. Metall., 21*, 1475 (1987).
33. D.D. Johnson, P.E.A. Turchi, M. Sluiter, D.M. Nicholson, F.J. Pinski, and G.M. Stocks, in *Alloy Phase Stability and Design*, G.M. Stocks, D. Pope, and A. Giamei, Ed., MRS Symposia Proceedings No 186, Materials Research Society, Pittsburgh, 21 (1991); B.L. Gyorffy, D.D. Johnson, F.J Pinski, D.M. Nicholson, and G.M. Stocks, in *Alloy Phase Stability*, G.M. Stocks and A. Gonis, Ed., NATO ASI Series 163, Kluwer Academic Publishers, Dordrecht, The Netherlands, 421 (1989).
34. C. Wolverton, D. de Fontaine, and H. Dreyssé, *Phys. Rev. B, 48*, 5766 (1993).

35 Y. Wang, J.S. Faulkner, and G.M. Stocks, *Phys. Rev. Lett., 70*, 3287 (1993).

36. VL. Moruzzi, J.F. Janak, and A.R. Williams, *Calculated Electronic Properties of Metals*, Pergamon Press, Inc., New York (1978); *Electronic Structure, Dynamics, and Quantum Structural Properties of Condensed Matter*, J.T. Devreese and D. Van Camp, Ed., Plenum Publishing Corp , New York (1985).
37. P. Hohenberg and W. Kohn, *Phys Rev., 136*, B864 (1964).
38. W. Kohn and L.J. Sham, *Phys Rev., 140*, A1133 (1965).
39. O.K. Andersen, *Phys. Rev. B, 12*, 3060 (1975); E. Wimmer, H. Krakauer, M. Weinert, and A J. Freeman, *Phys. Rev. B, 24*, 864 (1981); D.R. Hamann, *Phys. Rev. Lett., 42*, 662 (1979); S.-H. Wei

and H. Krakauer, *Phys. Rev. Lett., 55*, 1200 (1985); S.-H. Wei, H. Krakauer, and M. Weinert, *Phys. Rev. B, 32*, 7792 (1985).
40. D.J. Singh, *Planewaves, Psuedopotentials, and the LAPW Method*, Kluwer Academic Publishers, Boston (1994).
41. J.M. Sanchez, F. Ducastelle, and D. Gratias, *Physica A, 128*, 334 (1984); J.M. Sanchez, *Phys. Rev. B, 48*, 14013 (1993).
42. R. Kikuchi, *Phys. Rev., 81*, 988 (1951).
43. K. Binder and D.W. Heermann, *Monte Carlo Simulations in Statistical Physics*, Springer-Verlag, Berlin (1988).
44. N. Metropolis et al., *J. Chem. Phys., 21*, 1087 (1953).
45. Z.W. Lu, D.B. Laks, S.-H. Wei, and A. Zunger, *Phys. Rev. B, 50*, 6642 (1994).
46. J.M. Cowley, *J. Appl. Phys., 21*, 24 (1950).
47. Z.W. Lu and A. Zunger, *Phys. Rev. B, 50*, 6626 (1994)
48. Z.W. Lu, S.-H. Wei, A. Zunger, S. Frota-Pessoa, and L.G. Ferreira, *Phys. Rev. B, 44*(2), 512-544 (1991).
49. E. Wigner, *Phys. Rev., 46*, 1002 (1934).
50. D.M. Ceperley and B.J. Alder, *Phys. Rev. Lett., 45*, 566 (1980).
51. J.P Perdew and A. Zunger, *Phys. Rev., B, 23*, 5048 (1981).
52. H.J. Monkhorst and J.D. Pack, *Phys. Rev. B, 13*, 5188 (1976).
53. Z.W. Lu, S.-H. Wei, and A. Zunger, *Europhys. Lett., 21*, 221-226 (1993).
54. R. Magri, S.-H. Wei, and A. Zunger, *Phys. Rev. B, 42*(17), 11388-11391 (1990).
55. C. Wolverton and A. Zunger, unpublished.
56. K.M. Myles, *Metall. Trans. AIME, 242*, 1523 (1968).
57. L.G. Ferreira, A.A. Mbaye, and A. Zunger, *Phys. Rev. B, 35*, 6475 (1987); *Phys. Rev. B, 37*, 10547 (1988).
58. J.W.D. Connolly and A.R. Williams, *Phys. Rev. B, 27*, 5169 (1983).
59. G.M Kuznetsov, E.I. Rytvin, and I.V. Nikomova, *Izv. Akad. Nauk SSSR, Met., 4*, 194-197 (1985) in Russian; TR: *Russ. Metall., 4*, 189-192 (1984).
60. A.K. Niessen, F.R. de Boer, R. Boom, P.F. de Chatel, W.C.M. Mattens, and A.R. Miedema, *Calphad, 7*(1), 5 1-70 (1983).
61. V. Gerold and J. Kern, *Acta Metall., 35*, 393 (1987).